# MESH QUALITY CONTROL FOR INDUSTRIAL NAVIER-STOKES PROBLEMS VIA A POSTERIORI ERROR ESTIMATES

R. E. BANK*, J. CAO†, B. MANTEL‡, AND J. PÉRIAUX§

**Abstract.** The main goal of this paper is to study adaptive mesh techniques, using a posteriori error estimates, for the finite element solution of the Navier-Stokes equations modeling steady and unsteady flows of viscous fluids. Among existing operator splitting techniques, the $\theta$-scheme is used for time integration of the Navier-Stokes equations. Then a posteriori error estimates, based on the solution of a local system for each triangular element, are derived in the framework of the generalized Stokes problem. Adaptive strategies, including hierarchical and non-hierarchical refinements, and also enhanced by a moving mesh procedure, are developed to implement this mathematical criterion. Numerical simulations of viscous flows of industrial interest around aerodynamic shapes are presented and discussed to demonstrate the accuracy and efficiency of our methodology.

**Key words.** Navier-Stokes equations; generalized Stokes problem; a posteriori error estimates; mesh adaptive techniques.

**1. Introduction.** In the numerical simulation fluid flows, much attention has been paid to the Navier-Stokes equations because of their dominant role in the modelization of complex flows. When using finite element discretizations, adaptive grid generation methods, such as refinement, unrefinement, and mesh moving are attractive, allowing for an economical as well as accurate solution (cf. [4]).

The two main issues (cf. [2]) arising in connection with adaptive algorithms are: first, how to determine where adaptive remeshing is needed, and second, the choice of the particular adaptive procedure to be used.

In addressing the first issue, three main approaches have been studied. The first is to use a purely geometric criterion: one can choose triangles with poor geometric quality, and then modify the locations of some mesh points in order to move these triangles closer to the ideal of equilateral triangles. If only interpolation errors need to be minimized, this approach explicitly provides a priori estimates (cf. [16]) and yields an isotropical mesh well suited to simulating non-directional flows.

The second possibility is to use a physical criterion: here one creates a function based on the physical variables of the model equations. The goal is to capture important physical properties in some existing computation cases (cf. [19], [21], [13] and [24], for example). Unfortunately, an ideal physical criterion might be sensitive to many problem specific factors, which must be tuned on an ad hoc basis for each new application.

The third approach is a mathematical criterion based on a posteriori estimates. Here one estimates the errors within each element by solving a local Neumann problem corresponding to the mathematical model. Through solving this local Neumann problem, we obtain the a posteriori error estimates, which can be used to form both local and global energy norms involving all the physical variables. This energy norm is ultimately used to approximately equi-distribute the error index over the mesh. This methodology is general in its approach; the error estimator can be computed for all problems governed by the same mathematical model. In this study, we adopt

*Department of Mathematics, University of California, San Diego (*UCSD*), La Jolla, CA 92093;
†Department of Mathematics, University of California, San Diego (*UCSD*), La Jolla, CA 92093;
‡Dassault Aviation DGT/DEA B.P. 300 92214 St Cloud Cedex France;
§Dassault Aviation DGT/DEA B.P. 300 92214 St Cloud Cedex France.

mainly this mathematical viewpoint with the former two approaches appropriately taken into account.

Historically, this mathematical approach was introduced by Babuška for more general problems (cf. [3]); in the domain of elliptic equations, some theoretical research results of a posteriori error estimates can be found also in [5], [11]. Then, some analyses on this topic were carried out in [26] in the case of the primitive Stokes problem. Also in this direction, we can find in [15] the research results extended to the compressible generalized Stokes problem and their application to the case of the incompressible Navier-Stokes equations.

Concerning the second principal issue, we have experimented with all the mesh adaptive techniques appearing in different versions of $PLTMG$. These include the refinement and unrefinement of triangles in a nested way (cf. [6]), resulting in an obvious hierarchical structure in the adapted mesh. We have also tried a more recently implemented "bisection refinement" algorithm (cf. [8]) in which the parent-child relation among elements no longer exists on the triangulation and the granularity of the adapted grid looks quite continuous. In addition to refinement/unrefinement, we can move points on the mesh within a reasonably closed zone to further improve the mesh quality (cf. [7], [10]). The refinement/unrefinement and moving mesh techniques complement each other, allowing for great flexibility to achieve the best mesh possible.

The rest of the paper is organized as follows. In Section 2, we present the mathematical models of the Navier-Stokes problem and its linear subproblem, the maximally generalized Stokes problem (also called the "compressible" generalized Stokes problem). Then we consider in this section some stability issues arising in connection with the finite elements discretizations using the famous "mini-element" and Petrov-Galerkin formulations. In Section 3, we give the framework of a posteriori error estimate computations corresponding to the compressible generalized Stokes problem and the incompressible Navier-Stokes problem, respectively. Guided by this mathematical approach, we outline different mesh adaptation schemes in Section 4. The practical applications of our mesh quality control techniques are demonstrated in Section 5. Various selected test cases have been implemented, concerning both generalized Stokes flows and Navier-Stokes flows, and using several kinds of mesh adaptive techniques. Finally, we make some concluding remarks in Section 6.

## 2. (Navier - )Stokes problems.

**2.1. Mathematical modeling of (Navier - )Stokes flows.** To analyze the behavior of a fluid around or inside a given domain, basically the Navier-Stokes equations have to be solved. If we treat the problems under the hypothesis of incompressibility, with $\Omega$ and $\Gamma$ denoting the computational domain ($\Omega \subset \mathbb{R}^N, N = 2, 3$ in practice) and its boundary, respectively, the flow is governed by the following *incompressible Navier-Stokes equations*:

$$\frac{\partial \vec{u}}{\partial t} - \nu \Delta \vec{u} + (\vec{u} \cdot \vec{\nabla})\vec{u} + \vec{\nabla} p = \vec{f} \qquad \text{in } \Omega \tag{2.1}$$

$$\vec{\nabla} \cdot \vec{u} = 0 \qquad \text{in } \Omega \tag{2.2}$$

where $\vec{u}, p$, and $\vec{f}$ represent the velocity, the pressure and the body force, respectively; the positive parameter $\nu$ is the reduced viscosity of the fluid.

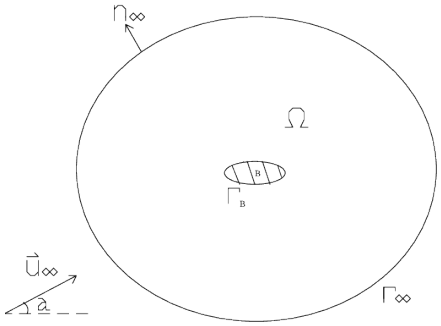


FIG. 2.1. *Computational domain.*

Boundary conditions need to be added. For example, in the case of the aerofoil of Fig. 2.1, because of viscosity, we use the following adherence condition:

$$\vec{u} = \vec{0} \qquad \text{on } \Gamma_B = \partial B \tag{2.3}$$

and the conditions at infinity are typically imposed by:

$$\vec{u} = \vec{u}_\infty \qquad \text{on } \Gamma_\infty \tag{2.4}$$

with $\vec{u}_\infty$ given. If $\Omega$ is a bounded region, standard boundary conditions are:

$$\vec{u} = \vec{g} \qquad \text{on } \Gamma \tag{2.5}$$

where the function $\vec{g}$ should satisfy:

$$\int_\Gamma \vec{g} \cdot \vec{n} \; ds = 0 \tag{2.6}$$

with $\vec{n}$ the outward unit vector normal to $\Gamma$. (2.6) is consistent with the continuity condition of the incompressible fluid.

Finally, for the time-dependent problem (2.1)-(2.2), an initial condition such as

$$\vec{u}(x, 0) = \vec{u}_o(x) \qquad \text{in } \Omega \tag{2.7}$$

with $\vec{u}_o$ given, is usually prescribed.

The principle difficulties in numerically solving the Navier-Stokes equations are the nonlinearity due to the convection term $(\vec{u} \cdot \vec{\nabla})\vec{u}$, the incompressibility condition $\vec{\nabla} \cdot \vec{u} = \vec{0}$, which usually restricts the applicability of numerical approaches, and the coupling of these two difficult points within the system of equations. Using convenient operator splitting methods for the time discretization of the Navier-Stokes equations, we are able to decouple the effects associated with the nonlinearity and incompressibility, respectively. Among different operator splitting techniques, the $\theta$-scheme (cf. [17]) can reach a precision of order 2 in time. With this approach, for each interval of integration $[n\Delta t, (n+1)\Delta t](n = 0, 1, 2, ...)$, let $\theta \in [0, 1/2]$, and then we divide this interval into three subintervals and correspondingly obtain the following three subproblems:

- $t \in [n\Delta t, (n+\theta)\Delta t]$ :

$$\left\{\begin{array}{ll} [\vec{u}^{n+\theta} - \vec{u}^{n}]/[\theta\Delta t] - a\nu\Delta\vec{u}^{n+\theta} + \vec{\nabla}p^{n+\theta} & \\ = \vec{f}^{n+\theta} + b\nu\Delta\vec{u}^{n} - (\vec{u}^{n}\cdot\vec{\nabla})\vec{u}^{n} & \text{in } \Omega \\ & \\ \vec{\nabla}\cdot\vec{u}^{n+\theta} = 0 & \text{in } \Omega \\ \vec{u}^{n+\theta} = \vec{g}^{n+\theta} & \text{on } \Gamma \end{array}\right. \tag{2.8}$$

- $t \in [(n+\theta)\Delta t, (n+1-\theta)\Delta t]$ :

$$\left\{\begin{array}{ll} [\vec{u}^{n+1-\theta} - \vec{u}^{n+\theta}]/[(1-2\theta)\Delta t] - b\nu\Delta\vec{u}^{n+1-\theta} + (\vec{u}^{n+1-\theta}\cdot\vec{\nabla})\vec{u}^{n+1-\theta} & \\ = \vec{f}^{n+1-\theta} + a\nu\Delta\vec{u}^{n+\theta} - \vec{\nabla}p^{n+\theta} & \text{in } \Omega \\ & \\ \vec{u}^{n+1-\theta} = \vec{g}^{n+1-\theta} & \text{on } \Gamma \end{array}\right. \tag{2.9}$$

- $t \in [(n+1-\theta)\Delta t, (n+1)\Delta t]$ :

$$\left\{\begin{array}{ll} [\vec{u}^{n+1} - \vec{u}^{n+1-\theta}]/[\theta\Delta t] - a\nu\Delta\vec{u}^{n+1} + \vec{\nabla}p^{n+1} & \\ = \vec{f}^{n+1} + b\nu\Delta\vec{u}^{n+1-\theta} - (\vec{u}^{n+1-\theta}\cdot\vec{\nabla})\vec{u}^{n+1-\theta} & \text{in } \Omega \\ & \\ \vec{\nabla}\cdot\vec{u}^{n+1} = 0 & \text{in } \Omega \\ \vec{u}^{n+1} = \vec{g}^{n+1} & \text{on } \Gamma \end{array}\right. \tag{2.10}$$

where $a = (1-2\theta)/(1-\theta), b = 1-a$ with the optimal value of $\theta : \theta = 1 - \sqrt{2}/2$ (cf. [14]).

Equation (2.9) is a nonlinear subproblem, denoted the *convection-diffusion problem*. The other two linear subproblems (2.8) and (2.10) are of the same type. They are special cases of the *generalized Stokes problem*:

$$\left\{\begin{array}{ll} \alpha\vec{u} - \nu\Delta\vec{u} + \vec{\nabla}p = \vec{f} & \text{in } \Omega \\ \vec{\nabla}\cdot\vec{u} = 0 & \text{in } \Omega \\ \vec{u} = \vec{g} & \text{on } \Gamma \end{array}\right. \tag{2.11}$$

For the flow of a compressible viscous fluid, two more variables, the density $\rho$ and the temperature $T$ should be considered. Therefore, the compressible Navier-Stokes problem is a more complicated system of equations than the previous incompressible case. Written in non-conservative form (cf. [13]) and discretized with the application of $\theta$-scheme, the compressible Navier-Stokes equations are split into three subproblems (cf. [23]), the first and the third of which (for $\vec{u}$ and $\rho$) are formally similar to (2.11) (for $\vec{u}$ and $p$) with a slight generalization (cf. [15]). They can be written as the following *compressible generalized Stokes problem*:

$$\left\{\begin{array}{ll} \alpha\vec{u} - \mu\Delta\vec{u} + \beta\vec{\nabla}\rho = \vec{f} & \text{in } \Omega \\ \beta\vec{\nabla}\cdot\vec{u} + \gamma\rho = h & \text{in } \Omega \\ \vec{u} = \vec{g} & \text{on } \Gamma \end{array}\right. \tag{2.12}$$

where $\alpha, \mu, \beta$ and $\gamma$ are all positive parameters.

**2.2. Space discretization.** For the generalized Stokes problem (2.11), the finite element discretization spaces for the velocity and the pressure need to satisfy the Ladyzhenskaya-Babuška-Brezzi (LBB) condition which guarantees the existence and

uniqueness of the solution of the discretized Stokes system. Among possible space discretizations satisfying the LBB condition, we choose the *"mini-element" formulation* (cf. [1]), which permits the resolution of the Stokes problem using a single grid for all the unknowns.

Let $\Omega_h$ be a standard finite element triangulation of the computational domain $\Omega$, with $h$ the granularity measure of the triangulation; the space of polynomials of degree $k$ is denoted as $P_k$. Then we define the following spaces:

$$H_h^1 = \{q_h \mid q_h \in C^o(\Omega),\ q_h \mid_\tau \in P_1,\ \forall \tau \in \Omega_h\} \tag{2.13}$$

$$W_{h_g}^1 = \{\vec{w}_h \mid \vec{w}_h \in (H_h^1)^2,\ \vec{w}_h \mid_\Gamma = \vec{g}\} \tag{2.14}$$

$$V_h^1 = \{\vec{v}_h \mid \vec{v}_h \in (C^o(\Omega))^2,\ \vec{v}_h \mid_\tau \in P_{1\tau}^* \times P_{1\tau}^*,\ \forall \tau \in \Omega_h\} \tag{2.15}$$

with

$$\begin{aligned} P_{1\tau}^* = \{ \quad & q \mid q = q_1 + \kappa\phi_\tau,\ q_1 \in P_1,\ \kappa \in \mathbb{R}, \\ & \phi_\tau \in P_3,\ \phi_\tau \mid_{\partial\tau} = 0,\ \phi_\tau(G_\tau) = 1 \ \} \end{aligned} \tag{2.16}$$

where $G_\tau$ is the centroid of the triangle $\tau$. A function like $\phi_\tau$ is usually called a *bubble-function*. Using the mini-element formulation ($\vec{u}_h \in V_h^1, \rho_h \in H_h^1$), the pressure is discretized by polynomials of degree 1 ($P1$), while the velocity is also discretized by polynomials of degree 1, augmented by a polynomial of degree 3 (bubble-function) which vanishes on the edges of the triangle $\tau$. In practice, we can eliminate the bubble unknowns in (2.12) using a static condensation technique (cf. [15]).

Another way to solve the Stokes problem on a single mesh is to modify the equations themselves so that the LBB condition is trivially satisfied. Inspired by the idea behind the original *Petrov-Galerkin formulation* (cf. [18]), we treat the compressible generalized Stokes problem (2.12) by adding a multiple of its first equation integrated against different kinds of test functions to both equations in this problem (cf. [15]), obtaining the following system [1]:

$$\left\{ \begin{array}{l} \text{Find } (\vec{u}_h, \rho_h) \in W_{h_g}^1 \times H_h^1 \text{ such that} \\ \quad \alpha(\vec{u}_h, \vec{v}) + \mu(\vec{\nabla}\vec{u}_h, \vec{\nabla}\vec{v}) - \beta(\rho_h, \vec{\nabla}\cdot\vec{v}) \\ \quad - \sum_{\tau\in T} \alpha\lambda_\tau(\alpha\vec{u}_h + \beta\vec{\nabla}\rho_h, \vec{v})_\tau \\ = (\vec{f}, \vec{v}) - \sum_{\tau\in T} \alpha\lambda_\tau(\vec{f}, \vec{v})_\tau \qquad \forall \vec{v} \in W_{h_o}^1 \\ \\ \quad -\beta(\vec{\nabla}\cdot\vec{u}_h, q) - \gamma(\rho_h, q) - \sum_{\tau\in T} \beta\lambda_\tau(\alpha\vec{u}_h + \beta\vec{\nabla}\rho_h, \vec{\nabla}q)_\tau \\ = -(h, q) - \sum_{\tau\in T} \beta\lambda_\tau(\vec{f}, \vec{\nabla}q)_\tau \qquad \forall q \in H_h^1 \end{array} \right. \tag{2.17}$$

Here, $(\cdot,\cdot)$ represents the usual inner product, $\lambda_\tau$ is a positive multiple for each triangle $\tau$. The terms added to the second equation of (2.17) stabilize the above system; by also modifying the first equation [2], the stiffness matrix of the whole system (2.17) becomes symmetric. If we set:

$$\lambda_\tau = \left(\frac{10}{7}\alpha + 5\mu\frac{h_1^2 + h_2^2 + h_3^2}{|\tau|^2}\right)^{-1} \tag{2.18}$$

[1] The Laplacian term in the first equation of (2.12) does not appear in (2.17) because $\Delta\vec{u}_h = \vec{0}$ when using linear interpolation functions over $\tau$.

[2] The setting of $\alpha$ and $\beta$ respectively to the stabilization terms in the two equations of (2.17) is used to symmetrize the whole system.

with $h_i$ $(1 \leq i \leq 3)$ and $|\tau|$ the length of three edges and the area of the triangle $\tau$, respectively, the unique solvability of (2.17) can be easily proved. In fact, this choice of $\lambda_\tau$ leads to the equivalence of the Petrov-Galerkin formulation and the mini-element formulation for the compressible generalized Stokes problem (cf. [15]).

We end this subsection with an important remark. From (2.12), we notice that the term $\gamma\rho$ appearing in the second equation seems to be stabilizing, leading some to try discretizing both the density $\rho$ and the velocity $\vec{u}$ with the simplest $P1$ functions (cf. [13], [23]). Unfortunately, this discretization is unable to overcome the density oscillation phenomenon when using economical iterative methods. In our numerical experiments presented in Section 5, we will show that even the standard Petrov-Galerkin and mini-element formulations are still inadequate to completely remove the oscillation of density, especially in the case of complicated geometries. However, when we add a stabilization term of the form $-\beta^2\lambda_\tau\eta(\vec{\nabla}\rho_h, \vec{\nabla}q)_\tau$, with $\eta$ a reasonable positive constant, to each triangle $\tau$ on the left-hand side of the second equation in (2.17) [3], the solution becomes more regular and acceptable. Because of the equivalency of the mini-element formulation to the Petrov-Galerkin formulation, one can apply the same idea to the mini-element formulation (cf. [8]) - just for the second equation in (2.12), in order to enhance the stabilization. So we find that this technique of increasing "artificial stability" is of great use in practice.

**2.3. Solvers.** As shown in (2.8)-(2.10), the Navier-Stokes equations can be separated into two kinds of subproblems using an operator splitting method.

The linear problem, i.e., the generalized Stoke problem, is solved by a multigrid algorithm with hierarchical basis (cf. [9]). In fact, if hierarchical refinements are used, the level-by-level mesh adaptation can provide us a natural family of nested triangulations. On the other hand, when we adopt the new version ($PLTMG$ 7.5) with non-hierarchical refinements, an auxiliary process can help us construct an "artificial multigrid" structure on an arbitrary mesh according to the distribution of granularity of the triangulation (cf. [12]). With transitions within $V$-cycle multigrid structure, a UZAWA-like conjugated gradient method is used to solve the whole Stokes system (cf. [26]).

Concerning the resolution of the nonlinear subproblem, i.e., the convection-diffusion problem (2.9), among the various numerical methods, let us mention the two main powerful strategies. First, we can transform the nonlinear equation into a least-squares problem, for which a conjugated gradient algorithm can be used to minimize the obtained functional. Otherwise, more generally, we can choose the GMRES (generalized minimal residual) algorithm in its nonlinear version to solve the resulting convection-diffusion problem (2.9). The details of both methods used in our work can be found in [15].

## 3. A posteriori error estimates.

**3.1. The compressible generalized Stokes problem.** Concerning a posteriori error estimation, our focus here is on the generalized Stokes problem in its most general form allowing us to extend the result to the practical solution of the Navier-Stokes equations. Here space does not allow for a complete derivation or detailed analysis of our estimates. The interested reader is referred to [15] for more details.

Our a posteriori error estimator requires the element-by-element solution of a local Neumann problem, discretized using finite elements of higher order, to obtain a local

[3] For the model of Stokes problem, we can approximately think $\vec{\nabla}\rho = 0$ at infinity.

error indicator for each physical variable $\vec{u}$ and $\rho$ in the compressible generalized Stokes problem (2.12). Let $B_\tau$ be the set of quadratic polynomials over $\tau$ which are zero at the vertices of $\tau$. Because in Section 2 we solve the (Navier-)Stokes problems using linear elements [4], the local error approximations should be computed with at least the "bump" basis functions constructed in $B_\tau$. Then, we can obtain $(\vec{e}_S, \varepsilon_S) \in (B_\tau)^3$, the local approximate error estimates of $(\vec{u}, \rho)$, by solving the following equation for each triangle $\tau$:

$$B\left((\vec{e}_S, \varepsilon_S), (\vec{v}, q)\right)_\tau = L\left((\vec{v}, q)\right)_\tau, \qquad \forall\ (\vec{v}, q) \in (B_\tau)^3 \tag{3.1}$$

Here, the two forms in (3.1) are written respectively as:

$$\begin{aligned} B((\vec{e}, \varepsilon), (\vec{v}, q))_\tau = \ & \alpha(\vec{e}, \vec{v})_\tau + \mu(\vec{\nabla}\vec{e}, \vec{\nabla}\vec{v})_\tau - \beta(\varepsilon, \vec{\nabla}\cdot\vec{v})_\tau + \beta(q, \vec{\nabla}\cdot\vec{e})_\tau \\ & + \gamma(\varepsilon, q)_\tau + \lambda_\tau(\alpha\vec{e} - \mu\Delta\vec{e} + \beta\vec{\nabla}\varepsilon, \beta\vec{\nabla}q - \alpha\vec{v})_\tau \end{aligned} \tag{3.2}$$

$$\begin{aligned} L\left((\vec{v}, q)\right)_\tau = \ & -\alpha(1-\alpha\lambda_\tau)(\vec{u}_h, \vec{v})_\tau - \mu < \vec{\nabla}\vec{u}_h, \vec{\nabla}\vec{v} >_\tau + \beta(\rho_h, \vec{\nabla}\cdot\vec{v})_\tau \\ & + \alpha\beta\lambda_\tau(\vec{\nabla}\rho_h, \vec{v})_\tau + < \mu[\tfrac{\partial\vec{u}_h}{\partial n}]_A - \beta\rho_h\vec{n}, \vec{v} >_{\partial\tau} \\ & + (1-\alpha\lambda_\tau)(\vec{f}, \vec{v})_\tau + (h, q)_\tau - \beta(q, \vec{\nabla}\cdot\vec{u}_h)_\tau - \gamma(q, \rho_h)_\tau \\ & - \alpha\beta\lambda_\tau(\vec{u}_h, \vec{\nabla}q)_\tau - \beta^2\lambda_\tau(\vec{\nabla}\rho_h, \vec{\nabla}q)_\tau + \beta\lambda_\tau(\vec{f}, \vec{\nabla}q)_\tau \end{aligned} \tag{3.3}$$

with $(\vec{u}_h, \rho_h)$, the numerical solution using either the mini-element formulation (using only the linear part for the velocity) or the Petrov-Galerkin formulation (2.17). In (3.2) and (3.3), the notation of $(\cdot,\cdot)_\tau$ is used as in (2.17) but strictly over triangle $\tau$ while $< \cdot, \cdot >_{\partial\tau}$ represents the inner product along the boundary of $\tau$; $[\frac{\partial\vec{u}_h}{\partial n}]_A$ is the average normal derivative of $\vec{u}_h$ across the edges of $\tau$; $\lambda_\tau$ keeps the same value as in (2.18).

Finally, using these local error indicators, we can form both local and global energy norms:

$$|||(\vec{e}, \varepsilon)|||^2 = \alpha\|\vec{e}\|^2 + \mu\|\vec{\nabla}\vec{e}\|^2 + (\gamma + \frac{\beta^2}{\mu})\|\varepsilon\|^2 \tag{3.4}$$

for use in our adaptive mesh algorithms.

**3.2. The incompressible Navier-Stokes problem.** The study on the generalized Stokes problem serves mainly for the resolution of Navier-Stokes equations. As first step, we present a practical application to the incompressible Navier-Stokes problem. In this case, $\beta = 1, \gamma = 0, h = 0, \mu = \nu$ and the density $\rho$ is now interpreted as the pressure $p$.

Because of nonlinearity, it is difficult to directly compute an error estimate for the Navier-Stokes equations. However, once operator splitting techniques are used, the complicated Navier-Stokes equations are decoupled into several subproblems, at least one of which corresponds well to the generalized Stokes problem (for example, both (2.8) and (2.10) in our paper). In this sense, it is suggested that the nonlinear term $(\vec{u}\cdot\vec{\nabla})\vec{u}$ be simply included into the residual on the right-hand side (cf. [25]). This treatment makes it possible to compute the errors of the solution of the Navier-Stokes equations within the generalized Stokes problem context but with a more complicated right-hand side.

[4] Even with the mini-element formulation, the velocity is represented by only its linear part after the static condensation of bubble unknowns.

The two equations in either (2.8) or (2.10) can more generally be expressed as:

$$
\left\{
\begin{array}{ll}
(\theta\Delta t)^{-1}\vec{u}^{\,+\theta} - a\nu\Delta\vec{u}^{\,+\theta} + \vec{\nabla}p^{+\theta} & \\
= \vec{f}^{\,+\theta} + (\theta\Delta t)^{-1}\vec{u} + b\nu\Delta\vec{u} - (\vec{u}\cdot\vec{\nabla})\vec{u} & \text{in } \Omega \\
 & \\
\vec{\nabla}\cdot\vec{u}^{\,+\theta} = 0 & \text{in } \Omega
\end{array}
\right. \tag{3.5}
$$

with the index $+\theta$ denoting advanced time $\theta\Delta t$, and $a, b$, $\theta$, the coefficients in the $\theta$-scheme described in Section 2.1. In our study, we will interpret the above linear subproblem resulting from the time-dependent Navier-Stokes equations as the following pure generalized Stokes problem:

$$
\left\{
\begin{array}{ll}
(\theta\Delta t)^{-1}\vec{u} - a\nu\Delta\vec{u} + \vec{\nabla}p = \vec{F} & \text{in } \Omega \\
\vec{\nabla}\cdot\vec{u} = 0 & \text{in } \Omega
\end{array}
\right. \tag{3.6}
$$

In other words, from (3.5) to (3.6), all the terms which appear in the right-hand side of either (2.8), (2.10), or (3.5) are here denoted by $\vec{F}$, which is substituted for $\vec{f}$ in (3.3) in our error estimate computation.

In addition, for the equation (3.1), in order to make the bilinear form (3.2) symmetric, we discard the terms $-\lambda_\tau a\nu\big(\Delta\vec{e}, \vec{\nabla}q - (\theta\Delta t)^{-1}\vec{v}\big)_\tau$ [5] to obtain a more economical estimator. Up to now, the approximate error estimate $(\vec{e}_{NS}, \varepsilon_{NS}) \in (B_\tau)^3$ of $(\vec{u}, p)$ in the environment of the Navier-Stokes problem can be defined by locally solving the following $9 \times 9$ linear symmetrical positive definite system:

$$
\left\{
\begin{array}{l}
(\theta\Delta t)^{-1}\big(1 - (\theta\Delta t)^{-1}\lambda_\tau\big)(\vec{e}_{NS}, \vec{\nabla}\vec{v})_\tau + a\nu(\vec{\nabla}\vec{e}_{NS}, \vec{\nabla}\vec{v})_\tau \\
-(\varepsilon_{NS}, \vec{\nabla}\cdot\vec{v})_\tau - (\theta\Delta t)^{-1}\lambda_\tau(\vec{\nabla}\varepsilon_{NS}, \vec{v})_\tau \\
= -a\nu(\vec{\nabla}\vec{u}_h, \vec{\nabla}\vec{v})_\tau + (p_h, \vec{\nabla}\cdot\vec{v})_\tau + (\theta\Delta t)^{-1}\lambda_\tau(\vec{\nabla}p_h, \vec{v})_\tau \\
+\big(1 - (\theta\Delta t)^{-1}\lambda_\tau\big)(\vec{f}, \vec{v})_\tau - \big(1 - (\theta\Delta t)^{-1}\lambda_\tau\big)\Big((\vec{u}_h\cdot\vec{\nabla})\vec{u}_h, \vec{v}\Big)_\tau \\
+ < a\nu[\frac{\partial\vec{u}_h}{\partial n}]_A - p_h\vec{n}, \vec{v} >_{\partial\tau} \qquad \forall\vec{v} \in (B_\tau)^2 \\
 \\
-(q, \vec{\nabla}\cdot\vec{e}_{NS}) - (\theta\Delta t)^{-1}\lambda_\tau(\vec{e}_{NS}, \vec{\nabla}q)_\tau - \lambda_\tau(\vec{\nabla}\varepsilon_{NS}, \vec{\nabla}q)_\tau \\
= (q, \vec{\nabla}\cdot\vec{u}_h) + \lambda_\tau(\vec{\nabla}p_h, \vec{\nabla}q)_\tau - \lambda_\tau(\vec{f}, \vec{\nabla}q)_\tau \\
+\lambda_\tau\Big((\vec{u}_h\cdot\vec{\nabla})\cdot\vec{u}_h, \vec{\nabla}q\Big)_\tau \qquad \forall q \in B_\tau
\end{array}
\right. \tag{3.7}
$$

where $(\vec{u}_h, p_h)$ is the current linear solution of the discrete generalized Stokes system from either one of (2.8) and (2.10). Since the above application concerns the incompressible Navier-Stokes equations, the energy norm should be correspondingly reduced into the following form:

$$
|||(\vec{e}, \varepsilon)|||^2 = \frac{1}{\theta\Delta t}\|\vec{e}\|^2 + a\nu\|\vec{\nabla}\vec{e}\|^2 + \frac{1}{a\nu}\|\varepsilon\|^2 \tag{3.8}
$$

**4. Adaptive mesh algorithms.** Recently we have been experimenting with several mesh refinement/unrefinement techniques, as well as mesh moving techniques.

The older of our mesh refinement/unrefinement techniques is based on the so called *regular refinement* of a given triangle into four similar triangles by pairwise connecting the midpoints. A simple example of this refinement scheme is given in

[5] The original form of these terms in (3.2) is $-\lambda_\tau\mu(\Delta\vec{e}, \beta\vec{\nabla}q - \alpha\vec{v})_\tau$.

Fig. 4.1. Nonuniform refinement using this scheme leads to the appearance of irregular nodes on the boundary of the refined region. Certain simple refinement rules [11] are used to control the distribution of irregular nodes. Additionally, this scheme allows elements with irregular nodes on the boundaries of the refined regions to be (temporarily) refined by simple bisection, called *green refinement*. Such green edges are removed at the beginning of each refinement step, and the original elements are then considered for regular refinement.

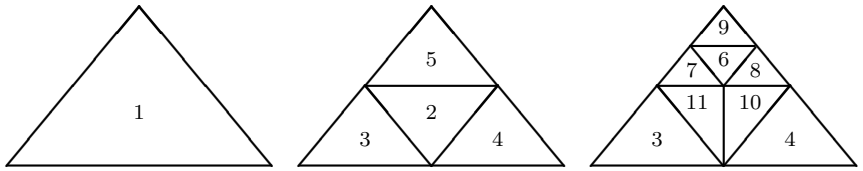


FIG. 4.1. *A simple triangle tree with three levels of refinement: elements 1 and 5 are regularly refined, while element 2 has green refinement.*

This refinement scheme yields good control of the shape regularity of all elements on the mesh, and allows for rapid transition from large to small elements near a singularity. The underlying data structure for this scheme is a *refined element tree*, with nodes on the tree corresponding to elements in the mesh, and using the obvious parent-child relations following directly from the refinement scheme. Such a tree imparts logical structure to the mesh, and allows for simple unrefinement (tree-pruning) algorithms, along with a structure which can be directly exploited by multilevel iterative solution techniques.

More recently, we have implemented a simple bisection algorithm (cf. [8]), called *longest edge bisection*, originally suggested by Rivara (cf. [22]). Elements selected for refinement are bisected along their longest edge. The neighbor element sharing the longest edge is also bisected along its longest edge. If the result is a triangulation (i.e. the longest edge for both elements is the same) the process stops. Otherwise, it is recursively applied to the longest edge neighbors of all refined elements. An example is shown in Fig. 4.2. This process is known to have finite termination, typically in a very small number of steps.

Although there is also a natural tree data structure which could be used in this case, we have implemented our longest edge bisection algorithm with no refinement tree, keeping only those elements which are currently in the mesh. This has allowed us to study coarsening algorithms for use on completely unstructured meshes. Such algorithms have application in the adaptive unrefinement of an unstructured mesh, as well as certain algebraic hierarchical basis multilevel iterative methods [12].

For both refinement and unrefinment algorithms, a posteriori error estimates are used to decide which elements to refine/unrefine. The guiding principle is that of *mesh equilibration*; that is, we attempt through the refinement/unrefinment process to create a final mesh in which all elements have approximately the same error regardless of size.

Our mesh moving algorithm also uses a posteriori error estimates, but in a slightly different fashion. In our algorithm, the mesh topology (connectivity) remains fixed, but the locations of the mesh points themselves are allowed to move in response to

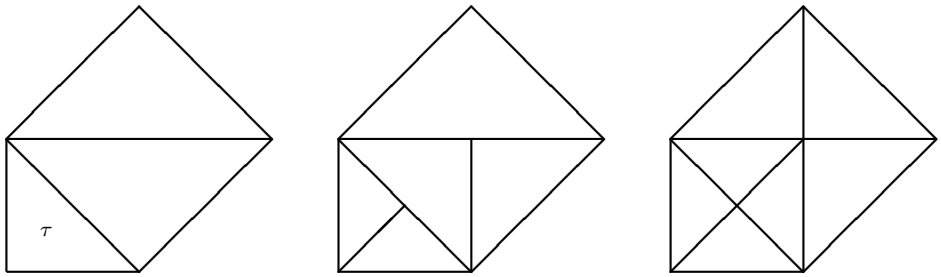


FIG. 4.2. *Element $\tau$ is refined by the longest edge bisection method: from the original mesh (left), the first step of bisection (middle) does not yield a compatible triangulation, however, the second step (right) does yield a triangulation.*

the error estimates. Our procedure consists of a Gauss-Seidel-like iteration on the vertices in the mesh, in which the position of each vertex is locally optimized with all other vertices held fixed. This is illustrated in Fig. 4.3, where the position of vertex $v$ is optimized within the region $\Omega_v$ by approximately minimizing the a posteriori error estimate with respect to vertex location. Each optimization problem has two degrees of freedom, and is solved using a simple approximate Newton iteration. Details of this algorithm can be found in [10]. Not all vertices in the mesh are allowed to move. Some boundary and interface vertices must remain fixed to preserve the definition of the region; others are allowed only one degree of freedom.

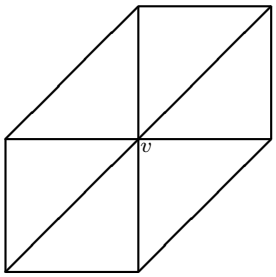


FIG. 4.3. *The subregion $\Omega_v$, associated with vertex $v$.*

## 5. Numerical experiments.

**5.1. Navier-Stokes flow simulations.** We first consider the solution of the Navier-Stokes equations for a steady flow of incompressible viscous fluid in a backward facing step. This test case is a quite classical and significant test problem for Navier-Stokes solvers and a workshop (cf. [20]) has been organized for this computation. In this work, we will use mesh adaptation guided by a posteriori error estimator analysis.

Initially, the channel is uniformly meshed with $NV = 599$, $NT = 756$ (see Fig. 5.1). As boundary conditions, $\vec{u}$ satisfies Poiseuille velocity profiles at the entrance

and exit of the channel and is $\vec{0}$ elsewhere on $\Gamma$. We take the height of the step as the characteristical length for Reynolds number calculation; in this test, we give $Re = 150$. The time step is set at $\Delta t = 0.1$.

FIG. 5.1. *Initial mesh of the channel.*

Using a posteriori error estimates and refining mesh in a nested way, we obtain a final mesh ($NV = 3729,\ NT = 6979$). On this mesh, the refinement is concentrated at the corner of enlargement and extends into the center of the flow, where the highest velocity occurs, as well as in the region of recirculation. Fig. 5.2 has grouped, from the top to the bottom, the enlarged final mesh, the associated iso-pressure lines, the recirculation detail and the iso-velocity-module distribution. In particular, the quite fine granularity around the corner of enlargement makes it possible to illustrate the flow separation phenomenon on this mesh. The geometrical average error value obviously decreases from the beginning ($\bar{e} = 0.497 \times 10^{-2}$) to the end ($\bar{e} = 0.241 \times 10^{-3}$). The intermediate steps in this test case are detailed in [15].

Next, we will present a numerical experiment of more industrial interest. It concerns the unsteady flow of incompressible fluid, governed also by the Navier-Stokes equations, around a stylized air inlet with a high incidence: $\alpha = 40^o$. The boundary conditions are imposed in a standard way as described in Section 2.1, except that an internal suction phenomenon needs to be simulated to avoid a possible blockage and aspirate the vortex which is generated at the entrance of the air inlet. With the distance between the walls of the nozzle as characteristical length, the Reynolds number is $Re = 300$. In this case, we take $\Delta t = 0.03333$ for time integration.

We begin this test case from the coarse mesh ($NV = 638, NT = 1144$) first by an initialization of the Stokes solution (see Fig. 5.3). Then, at $t = 2/3, 4/3$ and 2.0, we refine mesh three times, also according to the a posteriori error estimate (3.7) and with the hierarchical refinements, and we get totally four successive meshes and the associated unsteady solution (see Fig. 5.4). Fig. 5.5 shows us the streamline and iso-pressure-line distributions on the whole computational domain at the final time $t = 8/3$.

From the displays in Fig. 5.4, we see that the error obtained by the a posteriori error estimate computation follows closely the time-dependent solution, consequently, the advancing refinement is concentrated in the zone of vortices and especially consolidated at the two leading edges of the two walls. This series of mesh refinements results in a considerable decrease of average error $\bar{e}$: from 0.482 on the coarse grid to

FIG. 5.2. *Final mesh and the associated solutions.*

$0.182 \times 10^{-3}$ on the final mesh (cf. [15]).

**5.2. Generalized Stokes flow simulations.** For the future application to the compressible Navier-Stokes problem, we next consider some examples of the compressible generalized Stokes problem. Here we use our more recent mesh refinement algorithm, and our adaptive moving mesh algorithm.

In this subsection, we will demonstrate two flow examples, both of which obey the generalized Stokes equations in (2.12) with $\alpha = 1.0, \mu = 0.01, \beta = 1.0, \gamma = 1.0, \vec{f} = \alpha\vec{u}_\infty, h = 0$ and standard boundary condition setting including (2.3) and (2.4); the attack angle is set at zero also for both.

Our first example is an academic test case. The initial mesh is symmetrically given with $NV = 96, NT = 160$. Then we set successively four target numbers of nodes: $NV_{target} = 200, 500, 750, 1000$, obtaining a final mesh with $NV = 1000, NT = 1892$.

FIG. 5.3. *Initial mesh and the associated streamlines of Stokes flow.*

Both the initial mesh and the final one are shown in Fig. 5.6.

We imposed some extra constraints (cf. [8]) on the adaptive process to insure symmetry in the mesh is preserved. This makes the final solution completely symmetric (see Fig. 5.7), which ideally corresponds to the real flow background.

With mesh adaptation in this test case, the errors goes down gradually; the indices of errors concerning the velocity part ($\sqrt{\alpha\|\vec{e}\|^2+\mu\|\vec{\nabla}\vec{e}\|^2}/\sqrt{\alpha\|\vec{u}\|^2+\mu\|\vec{\nabla}\vec{u}\|^2}$) and the density part ($\|\varepsilon\|/\|\rho\|$) are respectively demonstrated in Fig. 5.8.

Finally, a more sophisticated example in the compressible case is the flow around a three piece airfoil, within a circular domain.

The initial mesh for this domain has $NV = 523, NT = 902$ (see Fig. 5.9). Our final mesh, generated through several steps of mesh refinement and mesh moving, has $NV = 3597,\ NT = 6922$ (see Fig. 5.10).

For this problem, if we use either the mini-element formulation or the Petrov-Galerkin formulation in their original forms, the numerical solution of the density oscillates unacceptably near the bodies (see Fig. 5.11). However, if we modify the mini-element formulation or the Petrov-Galerkin formulation as described in Section 2.2 (in our case, $\eta = 4$), we can see from Fig. 5.12 that the oscillation phenomenon of the density completely disappears!

In addition, from Fig. 5.13, we study the details of the flow in the regions of slat-main-wing connection (left) and main-wing-flap connection (right). The numerical solution without oscillation shows the applicability and effectiveness of our augmented stabilization technique.

In Fig. 5.14, the performance shows us the errors on the decrease along with successive mesh adaptations; and the statistics demonstrate that CPU time cost for mesh adaptation remains at an acceptably low rate.

**6. Conclusion.** A posteriori error estimates, coupled with the application of different adaptive mesh techniques, permit an efficient and accurate finite element solution of the generalized Stokes problem as well as the Navier-Stokes problem even for complicated geometries, proving to be a valuable tool for obtaining a high quality

FIG. 5.4. *Evolution of the unsteady solution (streamline) with mesh adaptations (from the top to the bottom): (1) t= 2/3 on the level 1 mesh (NV=638, NT=1144); (2) t= 4/3 on the level 2 mesh (NV=806, NT=1442); (3) t= 2.0 on the level 3 mesh (NV=1538, NT=2824); (4) t= 8/3 on the level 4 mesh (NV=2855, NT=5360).*

FIG. 5.5. *Streamline and iso-pressure-line distributions at t=8/3 on the level 4 mesh.*

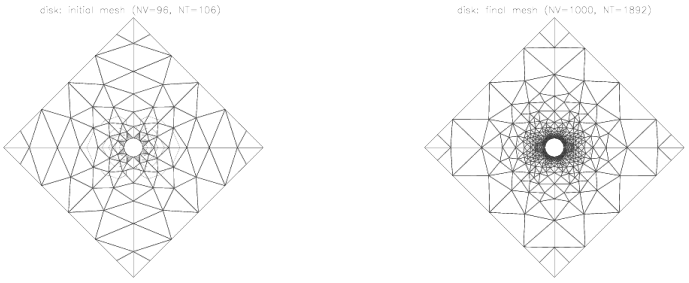


FIG. 5.6. *Initial and final meshes.*

numerical solution.

**7. Acknowledgements.** This work was partly supported by contract DRET 94-518 from Direction des Recherches Etudes et Techniques via Dassault Aviation. We wish to thank M. O. Bristeau, R. Glowinski, J. F. Maitre and O. Pironneau for their helpful advice during this study.

REFERENCES

[1] D. N. ARNOLD, F. BREZZI, AND F. FORTIN, *A stable finite element for the Stokes equations*, Calcolo, 21(4) (1984), pp. 337–344.

[2] I. BABUŠKA AND W. GUI, *Basic principles of feedback and adaptive approaches in the finite element method*, tech. rep., University of Maryland, 1985.

[3] I. BABUŠKA AND W. C. RHEINBOLDT, *A posteriori error estimates for the finite element method*, Int. J. Numer. Methods Eng., 12 (1978), pp. 1597–1615.

[4] I. BABUŠKA, O. C. ZIENKIEWICZ, J. R. GAGO, AND E. R. A. OLIVEIRA, *Accuracy estimates and adaptive refinements in finite element computations*, John Wiley, London, 1986.

[5] R. E. BANK, *Analysis of a local a posteriori error estimator for elliptic equations*, in Accuracy Estimates and Adaptivity in Finite Element Computations, (eds. I. Babuška, O. C. Zienkiewicz, and E. Arantes e. Oliveira), J. Wiley and Sons, New York, 1986, pp. 119–128.

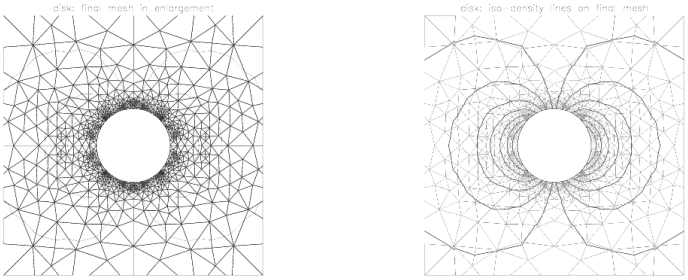


FIG. 5.7. *Final mesh and the associated iso-density lines (in enlargement).*

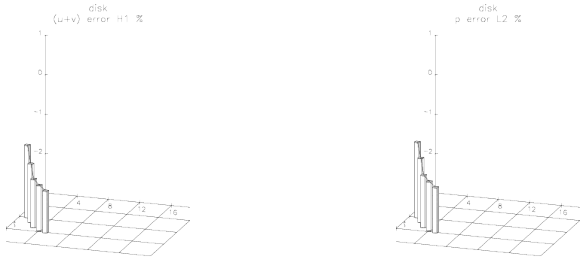


FIG. 5.8. *Behavior of* $\log_{10} \frac{||\vec{e}||_{H^1}}{||\vec{u}||_{H^1}}$ *(left) and* $\log_{10} \frac{||\varepsilon||_{L^2}}{||\rho||_{L^2}}$ *(right) as the mesh is refined.*

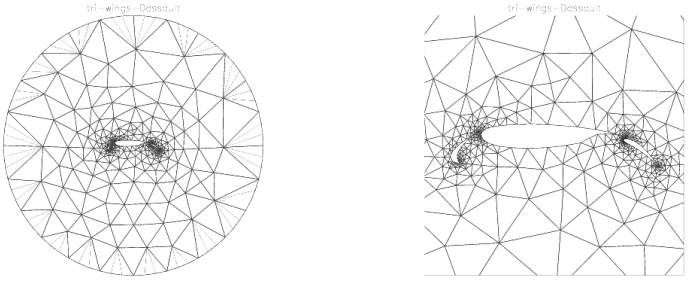


FIG. 5.9. *Initial mesh with enlargement.*

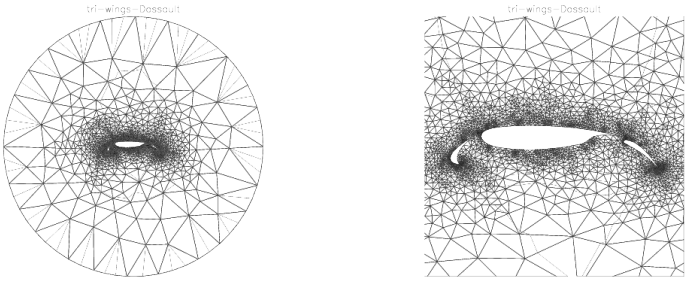


FIG. 5.10. *Final mesh with enlargement.*

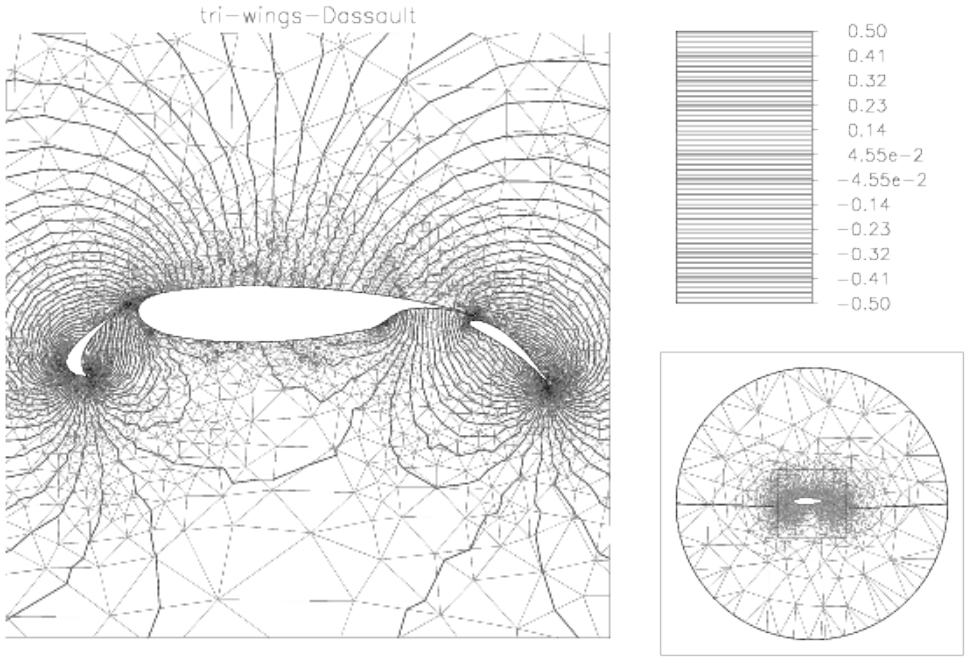


FIG. 5.11. *The solution resulting from the original mini-element formulation: 100 iso-density lines between -0.5 and 0.5.*

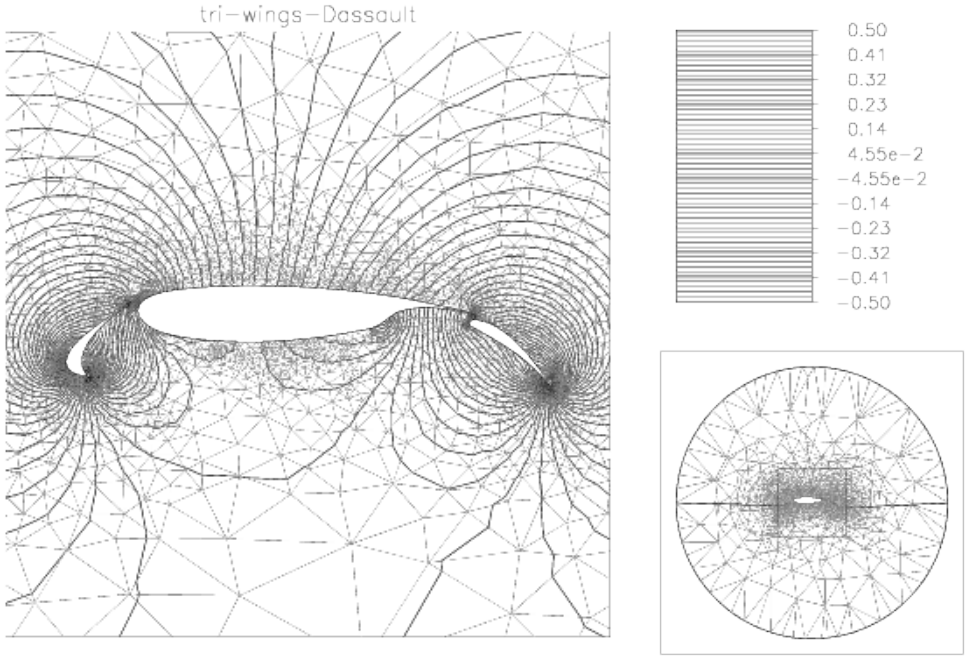


FIG. 5.12. *The solution resulting from the modified mini-element formulation: 100 iso-density lines between -0.5 and 0.5.*

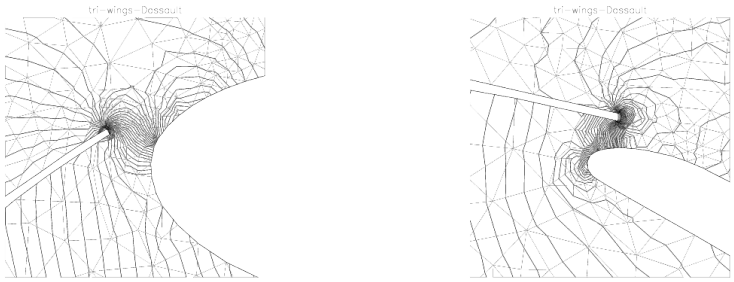


FIG. 5.13. *Detailed iso-density-line distribution in body-connection regions.*

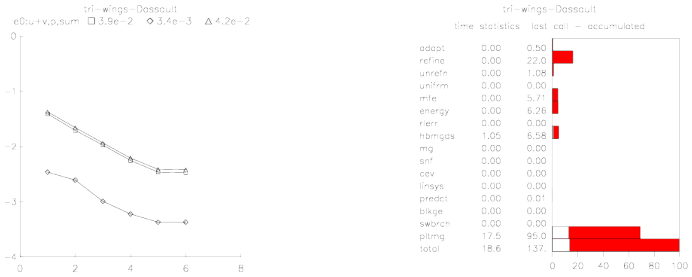


FIG. 5.14. *History of the errors (left) and CPU time statistics (right).*

[6] ———, *PLTMG: a software package for solving elliptic partial differential equations, Users' Guide 6.0*, Frontiers in Applied Mathematics, Vol. 7, SIAM, Philadelphia, 1990.

[7] ———, *PLTMG: a software package for solving elliptic partial differential equations, Users' Guide 7.0*, Frontiers in Applied Mathematics, Vol. 15, SIAM, Philadelphia, 1994.

[8] R. E. BANK, J. CAO, B. MANTEL, AND J. PÉRIAUX, *A non-hierarchical mesh adaptive algorithm for the generalized Stokes problem*, tech. rep., (to appear).

[9] R. E. BANK, T. F. DUPONT, AND H. YSERETANT, *The hierarchical basis multigrid method*, Numer. Math., 52 (1988), pp. 427–458.

[10] R. E. BANK AND R. K. SMITH, *Mesh smoothing using a posteriori error estimates*, SIAM J. Numerical Analysis, (to appear).

[11] R. E. BANK AND A. WEISER, *Some a posteriori error estimates for elliptic partial differential equations*, Mathematics of Computation, 44 (1985), pp. 283–301.

[12] R. E. BANK AND J. XU, *The hierarchical basis multigrid method and incomplete LU decomposition*, in Seventh International Symposium on Domain Decomposition Methods for Partial Differential Equations (D. Keyes and J. Xu, eds.), AMS, Providence, Rhode Island, 1994, pp. 163–173.

[13] M. O. BRISTEAU, R. GLOWINSKI, L. DUTTO, J. PÉRIAUX, AND G. ROGÉ, *Compressible viscous flow calculation using compatible finite element approximations*, Int. J. Numer. Meth. in Fluids, 11 (1990), pp. 719–749.

[14] M. O. BRISTEAU, R. GLOWINSKI, B. MANTEL, J. PÉRIAUX, AND P. PERRIER, *Numerical methods for incompressible and compressible Navier-Stokes problems*, in Finite element in fluids, # 6, John Wiley & Sons Ltd., 1985, pp. 1–40.

[15] J. CAO, *Estimations d'erreur a posteriori et techniques d'adaptation en éléments finis pour la simulation numérique d'écoulements de fluides visqueux*, Thèse de 3e cycle, Université Pierre et Marie Curie (Paris VI), France, 1995.

[16] P. G. CIARLET, *The finite element methods for the elliptic problems*, North-Holland Publishing Company, 1987.

[17] R. GLOWINSKI, *Numerical methods for nonlinear variational problems*, Springer-Verlag, New York, 1984.

[18] T. J. R. HUGHES, L. P. FRANCA, AND M. BALESTRA, *A new finite element formulation for computational fluid dynamics: V. Circumventing the Babuška-Brezzi condition: a stable Petrov-Galerkin formulation for the Stokes problem accommodating equal-order imterpo-*

*lations*, Comp. Meth. in Appl. Mech. and Engr., 59 (1986), pp. 85–99.

[19] R. Lohner, *Finite element for hyperbolic partial differential equations*, PhD thesis, University College of Swansea, 1984.

[20] K. Morgan, J. Périaux, and F. Thomasset(Eds.), *Analysis of laminar flow over a backstep facing step*, Notes on Numer. Fluid Mechanics, Vieweg, 1984.

[21] B. Palmerio and A. Dervieux, *Self adaptive F. E. M. algorithms for the Euler equations*, tech. rep., (Rapport de Recherche) INRIA $N^o$ 338, 1985.

[22] M. C. Rivara, *Algorithms for refining triangular grids suitable for adaptive and multigrid techniques*, J. Numer. Meth. Engrg., 20 (1984), pp. 745–756.

[23] G. Rogé, *Sur l'application et l'accélération de la convergence lors de la simulation numérique en éléments finis d'écoulements de fluides visqueux compressible*, Thèse de 3e cycle, Université Pierre et Marie Curie (Paris VI), France, 1990.

[24] M. G. Vallet, *Génération de maillages éléments finis anisotropes et adaptifs*, Thèse de 3e cycle, Université Pierre et Marie Curie (Paris VI), France, 1992.

[25] R. Verfürth, *A posteriori error estimator for the Stokes equations*, Numer. Math., 55 (1989), pp. 309–325.

[26] B. D. Welfert, *A posteriori error estimates and adaptive solution of fluid flow problems*, PhD thesis, University of California, San Diego, 1990.